

Optical and magneto-optical properties of nanocrystalline Fe-rich Fe-Si alloy films

Y. V. Kudryavtsev

Institute of Metal Physics, National Academy of Sciences of Ukraine, 36 Vernadsky Str, 03142, Kiev-142, Ukraine

Y. P. Lee*

Quantum Photonic Science Research Center and Department of Physics, Hanyang University, Seoul, 133-791, Korea

J. Dubowik

Institute of Molecular Physics, Polish Academy of Sciences, Smoluchowskiego 17, 60-179, Poznań, Poland

J. Y. Rhee

Department of Physics, Hoseo University, Asan, Choongnam, 336-795 Korea

(Received 26 February 2003; published 9 October 2003)

Magnetic, optical, and magneto-optical (MO) properties of nanocrystalline and amorphous $\text{Fe}_{1-x}\text{Si}_x$ ($0.0 \leq x \leq 0.5$) alloy films prepared by dc magnetron sputtering were investigated in the as-deposited state and after annealing at 710 K. The optical conductivity (OC) spectrum of amorphous $\text{Fe}_{0.51}\text{Si}_{0.49}$ alloy film shows a great resemblance to the OC spectrum of crystalline $\epsilon\text{-FeSi}$ ($B2$) which implies that the same type of short-range order is formed in this amorphous phase. All the crystalline $\text{Fe}_{1-x}\text{Si}_x$ alloy films with $0.30 \leq x \leq 0.49$ exhibit a prominent absorption peak near 2.5–3.1 eV. The MO responses for nanocrystalline $\text{Fe}_{1-x}\text{Si}_x$ alloy films ($0.21 \leq x \leq 0.30$) exceed those of pure Fe films. Such an enhancement is closely related to the interplay between the optical properties of Fe and $\text{Fe}_{1-x}\text{Si}_x$ alloy films.

DOI: 10.1103/PhysRevB.68.134416

PACS number(s): 75.70.-i, 75.50.Bb, 78.66.Bz, 78.20.Ls

I. INTRODUCTION

Since the discovery of the strong antiferromagnetic (AF) coupling in the Fe/Si multilayered films (MLF) a lot of efforts were devoted to understand its mechanism. If the spacer layer between Fe sublayer is not metallic, then the conventional theories of interlayer exchange coupling cannot be applied to this system and such a coupling must involve a novel mechanism. It is well known that Fe and Si produce a rich variety of stable bulk binary compounds:¹ nonmagnetic orthorhombic $\beta\text{-FeSi}_2$ (ξ phase), nonmagnetic FeSi with $B2$ type of structure (ϵ phase), ferromagnetic $\eta\text{-Fe}_5\text{Si}_3$ with Mn_5Si_3 type of structure and ferromagnetic Fe_3Si with a DO_3 structure and a negative heat of formation of 19.4 (ξ phase), 17.6 (ϵ phase), 11.7 (η phase), and 7.5 kcal/metal atom, respectively.² In addition to them several unstable compounds at room temperature (RT) are also mentioned to be grown. These include tetragonal metallic nonmagnetic $\alpha\text{-FeSi}_2$, a metastable metallic nonmagnetic FeSi with $B2$ structure, and hexagonal ferromagnetic metallic Fe_2Si (β phase).^{2,3} Therefore, it was hypothesized that a metallic metastable compound with $B2$ structure is spontaneously formed in the Fe/Si MLF during the deposition. By using a combination of soft-x-ray fluorescence and near-edge x-ray-absorption fine-structure spectroscopy,⁴ x-ray structural study,⁵ low-energy-electron diffraction, and Auger electron spectroscopy^{6,7} and cross-sectional transmission-electron microscopy⁸ it was confirmed that a metallic metastable compound with $B2$ structure is spontaneously formed in Fe/Si MLF during the deposition.

The conclusion on the metallic character of the spontaneously formed spacer between Fe sublayers in Fe/Si MLF with AF coupling was also made in our previous work on the basis of experimental and theoretical optical [and partially

magneto-optical (MO)] studies.⁹ Extracted contribution from the spacer to the total optical properties of the Fe/Si MLF mostly matched to the results of the first-principles calculations of the optical properties for the FeSi with $B2$ structure.⁹ The same approach was also employed by us to study the silicide formation in the Fe/Si MLF subjected to the ion-beam mixing.¹⁰ By comparing the experimental OC spectra with the theoretical ones of various Fe silicides and referring the results of magnetic measurements, we made the conclusion that the metastable Fe_2Si silicide at RT is formed owing to the ion-beam mixing on the top of such a MLF. However, these results were obtained by more or less indirect way. Therefore, it was interesting to grow such iron silicides and study experimentally their optical properties. If the metastable iron silicides are spontaneously formed between Fe and Si sublayers during the Fe/Si MLF deposition, it is natural to assume that this property may be used for the fabrication of pure silicide (without admixture of Fe) by choosing a proper sublayer thickness. However, it was not successful to fabricate these metastable silicides in this way.⁹

Some metastable phases of Fe-Si alloy phases can be obtained using a variety of techniques such as epitaxial-alloy-film growth, coevaporation, melt spinning, mechanical alloying, solid-state interdiffusion etc.^{11–14} In this work we employed the codeposition of Fe and Si to produce of Fe-Si alloy films having a gradual change of alloy composition along the substrate from Fe-rich to Si-rich ones, expecting that a proper composition will be reached in some place of substrate, and due to the negative heat of the formation of silicide and/or additional heat treatment, some stable or metastable iron silicides can be grown.

On the other hand, Zhou *et al.* reported that the iron-rich Fe-Si alloys exhibit a noticeable enhancement of about 40–50 % Kerr rotation in comparison with that for pure Fe

TABLE I. Parameters of prepared and investigated Fe-Si alloy films.

Sample No.	Alloy composition	Film thickness (nm)	Film structure (as deposited)	Film structure (after annealing)
1	Fe _{0.93} Si _{0.07}	417	cryst.	N/A
2	Fe _{0.92} Si _{0.08}	384	cryst.	N/A
3	Fe _{0.85} Si _{0.15}	182	cryst.	N/A
4	Fe _{0.79} Si _{0.21}	134	cryst.	N/A
5	Fe _{0.70} Si _{0.30}	137	amorphous ?	cryst.
6	Fe _{0.61} Si _{0.39}	117	amorphous	cryst.
7	Fe _{0.51} Si _{0.49}	135	amorphous	cryst.

film.¹⁵ However, without knowing the detailed optical properties of these alloys, such an enhancement is hard to understand. Unfortunately, the only accessible data are concerning mainly nonmagnetic and nonmetallic ϵ -FeSi and FeSi₂ silicides.¹⁶ To the best of our knowledge the optical and MO properties of neither FeSi (*B2*) nor Fe₂Si as-well as Fe-rich Fe-Si alloys were not experimentally investigated so far. Thus, the purpose of this work is to fabricate the iron-rich silicides and to experimentally study their optical and MO properties.

II. EXPERIMENTAL DETAILS

A set of Fe_{1-x}Si_x alloy films with $0 < x < 1$ have been prepared by the dc-magnetron face-to-face sputtering from Fe and Si targets onto glass substrates (25×120 mm² in size) held at RT. Because of the distance between two targets, a certain compositional gradient was maintained along the long side of the substrate. After deposition the film was cut into 12 pieces along the short side of substrate, and 12 alloy samples of different composition were obtained. The composition of each Fe_{1-x}Si_x alloy sample was determined at its central part by x-ray fluorescence. We concentrated our attention on the iron-rich and equiatomic iron silicides. Therefore, only Fe_{1-x}Si_x alloy films from the compositional region of $0 < x < 0.50$ were investigated. The parameters used in the preparation of the Fe_{1-x}Si_x alloy films are summarized in Table I. The structural characterization of Fe_{1-x}Si_x alloy films was performed by high-angle x-ray diffraction (XRD) with Co-*K α* and Cu-*K α* radiations. The magnetic properties [in-plane magnetization loops $M(H)$] were measured at RT and in a magnetic field of 1.5 T by using a vibrating sample magnetometer (VSM). Ferromagnetic resonance (FMR) spectroscopy at RT for in-plane and out-of-plane configurations was also employed for the magnetic study. The details of the measurements for the diagonal components of the dielectric function (DF) tensor ($\tilde{\epsilon}_{xx} = \tilde{\epsilon}_{yy} = \tilde{\epsilon}_{zz} = \epsilon = \epsilon_1 - i\epsilon_2$), optical conductivity [(OC) $\sigma = \epsilon_2 \times \omega / 4\pi$] and MO [equatorial Kerr effect (EKE) δ_p] can be found elsewhere.¹⁷ Since the compositional region of $0.30 \leq x < 0.50$ is the most appropriate one for the expected silicides formation, the Fe_{1-x}Si_x alloy films with $0.30 \leq x < 0.50$ were annealed at 710 K for 90 min in a high vacuum condition and then another complete set of measurements was repeated again.

III. RESULTS AND DISCUSSION

A. Structural and magnetic properties of the Fe_{1-x}Si_x alloy films

The XRD results are shown in Figs. 1 and 2. It is seen that the XRD spectra for Fe-rich alloys with $x = 0.07 \sim 0.15$ exhibit only one well-defined diffraction peak located rather near but not coincided with the (110)-peak position for bulk Fe and the most intense diffraction lines for several iron silicides. Further increase in Si content leads to the broadening of diffraction lines and to a rapid decrease in intensities. The diffraction peak position and its width were obtained by fitting the raw XRD curves with Lorentzian function. The obtained data were also used for the calculation of mean-grain size by using Debye-Sherrer formula. It is seen that the as-deposited Fe_{1-x}Si_x alloy films are nanocrystalline (or even amorphous for $x \geq 0.39$ where no XRD peaks were observed) with rather small mean grain size which strongly depends on the silicon content in alloy (see Fig. 2).

The interplanar spacings for $0.07 \leq x \leq 0.39$ determined from the diffraction peak position are nearly independent of x . This contradicts to the well-known compositional dependence of the (110) α -Fe interplanar spacing for bulk Fe-Si alloys which follows the Vegard's rule. (see Fig. 2). On the other hand, the theoretical lattice constant of Fe-Si solid solution is almost independent of the concentration of Si when $0 \leq x \leq 0.25$.¹⁸ At the same time, the application of the extended x-ray absorption fine structure spectroscopy (EXAFS) for the structural analyses of the Fe_{1-x}Si_x alloy films (0

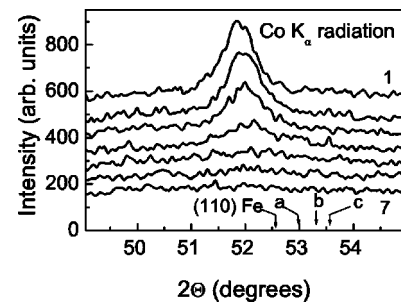


FIG. 1. High-angle XRD spectra for the as-deposited films. All curves are shifted upward with respect to the curve 7 for clarity. Arrows at the bottom indicate the location of the most intense diffraction peaks for bulk Fe, (a) ϵ -FeSi(110), (b) Fe₃Si(220), (c) Fe₂Si(110) (Refs. 2,29).

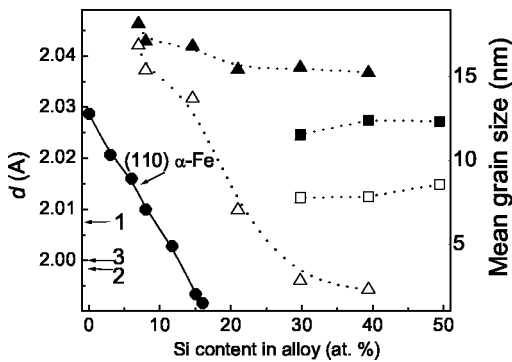


FIG. 2. Interplanar spacing (solid symbols) for the as-deposited (triangle) and annealed (square) $\text{Fe}_{1-x}\text{Si}_x$ alloy films (left scale). Dotted lines are for the guide to eyes only. Open symbols (right scale) show the compositional dependence of mean-grain size for the as-deposited (triangle) and annealed (square) states. Solid circles show compositional dependence of the (110) spacing for the α -Fe (Ref. 29). Arrows labeled by 1, 2 and 3 indicate the (210), (110), and (220) interplanar spacings for the ϵ -FeSi, Fe_2Si , and Fe_3Si , respectively (Ref. 29).

$<x < 0.50$) prepared by dc magnetron sputtering revealed that the substitution of Fe atoms by Si atoms within bcc structure of α -Fe is observed for $x \leq 0.3$ compositional region.¹⁴ According to the phase diagram of bulk Fe-Si alloys for $0.11 \leq x \leq 0.24$ an α_1 -phase (DO_3) is equilibrium at RT. However, because of a little difference in lattice constants of these phases (2.48 and 2.44 Å, respectively) probably they cannot be distinguished in the nanocrystalline Fe-Si alloy films. The formation of the structure with a local order close to Fe_5Si_3 phase in amorphous $\text{Fe}_{0.60}\text{Si}_{0.40}$ alloy films was also observed by Díaz *et al.*¹⁴

Annealing of the $\text{Fe}_{1-x}\text{Si}_x$ alloy films with $0.30 \leq x \leq 0.49$ results in crystallization with a mean grain size of about 7–8 nm and some shift of the diffraction peaks to the high-angle side (see Fig. 2). However, the location of these diffraction peaks is still far from the position of the most intense diffraction peaks for the possible iron silicides (see Fig. 2). Therefore, the results of XRD study do not allow us to confidently conclude that which kind of short-range order or local environment is formed in the annealed and particularly in the as-deposited $\text{Fe}_{1-x}\text{Si}_x$ alloy films.

Figure 3 present the results of the magnetic measurements for as-deposited and annealed $\text{Fe}_{1-x}\text{Si}_x$ alloy films. $M(H)$ curve for the $\text{Fe}_{0.79}\text{Si}_{0.21}$ alloy film (not shown) is nearly the same as the $\text{Fe}_{0.70}\text{Si}_{0.30}$ film. It is seen that the saturation magnetization M_s gradually and nearly linearly decreases with Si content. The observed $M_s(x)$ dependence for the as-deposited $\text{Fe}_{1-x}\text{Si}_x$ alloy films is in a good qualitative agreement with the well-known results for bulk Fe-Si alloys¹⁹ and experimental data of Zhou *et al.*²⁰ for the nanocrystalline $\text{Fe}_{1-x}\text{Si}_x$ alloys prepared by mechanical alloying, though the magnitude is slightly smaller. The compositional dependence of magnetization measured by VSM for the as-deposited $\text{Fe}_{1-x}\text{Si}_x$ alloy films also agrees with the results of the FMR measurements (not shown); the effective magnetization of the $\text{Fe}_{1-x}\text{Si}_x$ alloy films determined by the

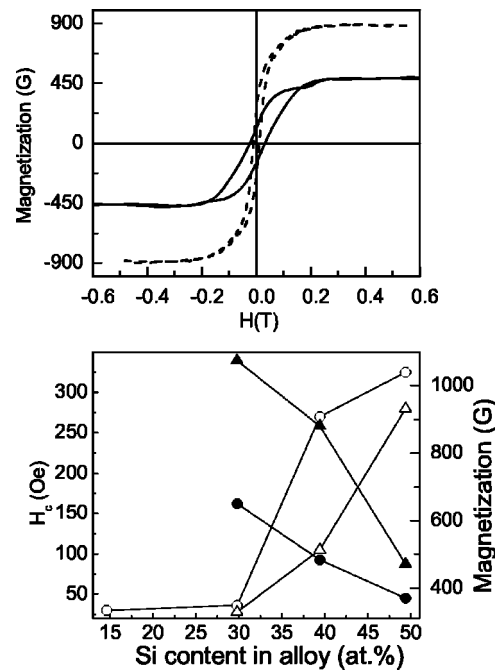


FIG. 3. Magnetization hysteresis loops for the as-deposited (solid lines) and annealed (dashed-dotted lines) $\text{Fe}_{0.61}\text{Si}_{0.39}$ alloy film (upper panel) and the compositional dependence of magnetization (right scale, solid symbols), and coercivity (left scale, open symbols) for the as-deposited (circles) and annealed (triangles) $\text{Fe}_{1-x}\text{Si}_x$ alloy films.

absorption-derivative positions as well as the peak intensity also decreases as the Si content increases.

It is known that bulk Fe-Si alloys are magnetically soft and have coercivities H_c of about 1 Oe. However, the coercivity of our as-deposited samples for $x \leq 0.30$ is noticeably larger (about 30 Oe). The softness of the nanocrystalline materials is related to low effective magnetostriction and small magnetocrystalline anisotropy due to random orientation of grains. Relatively high coercivity (for $x \leq 0.30$ region) may be related to the reduction of the magnetic-domain-wall mobility due to grain boundaries with a high stress and doping. For $x \geq 0.40$, H_c increases by about an order of magnitude (see Fig. 3). The same behavior was also observed by Varga *et al.*²¹ for the nanocrystalline $\text{Fe}_{1-x}\text{Si}_x$ alloys prepared by melt spinning and by Vélez *et al.* for amorphous $\text{Fe}_{1-x}\text{Si}_x$ alloy films prepared by dc magnetron sputtering.²² According to Varga *et al.*,²¹ in the $x \leq 0.30$ region the cubic phases (DO_3 and bcc) are dominant in the nanocrystalline $\text{Fe}_{1-x}\text{Si}_x$ alloys. Varga *et al.* relate the rapid growth of H_c for $x > 0.30$ to the appearance of the hexagonal η - Fe_5Si_3 phase, which is called a “killer” of soft magnetic properties.²¹ A strong decrease in the FMR line width observed for our $\text{Fe}_{1-x}\text{Si}_x$ alloy film with $x = 0.30$ in comparison with those with $x < 0.30$ can be explained in terms of small magnetic anisotropy of this alloy. This result nicely agrees with the well-known fact that $\text{Fe}_{0.70}\text{Si}_{0.30}$ alloy possesses the lowest magnetic anisotropy among the Fe-Si alloys. The increase in Si content in the as-deposited $\text{Fe}_{1-x}\text{Si}_x$ alloy films up to $x = 0.39$ causes significant broadening of the FMR absorption

line. Such a behavior also nicely corresponds to our magnetization data obtained by VSM (see Fig. 3).

Annealing of the $\text{Fe}_{1-x}\text{Si}_x$ alloy films ($x=0.30\sim 0.49$) results in noticeable changes of their magnetic properties in different ways for different samples even though the saturation magnetization increases by nearly two times for all samples (see Fig. 3). The coercivity for the annealed alloy films with $x=0.30$ and 0.49 are nearly the same as for as-deposited state, while H_c for annealed $\text{Fe}_{0.61}\text{Si}_{0.39}$ alloy film is reduced by more than 2 times in comparison with the as-deposited state. It is seen that the in-plane saturation magnetic field H_s for the annealed $\text{Fe}_{0.70}\text{Si}_{0.30}$ alloy film increases by nearly an order of magnitude, while for $\text{Fe}_{0.61}\text{Si}_{0.39}$ alloy film the opposite tendency is observed (see the upper panel of Fig. 3). On the other hand, H_s for the annealed $\text{Fe}_{0.51}\text{Si}_{0.49}$ alloy film is practically the same as for the as-deposited film. The changes in the magnetic properties (M_s and H_c) due to annealing of $\text{Fe}_{1-x}\text{Si}_x$ alloy films observed by VSM are similar to the changes in the FMR spectra. In-plane FMR absorption lines for all annealed films are shifted to the low-field region, indicating the enhancement of magnetization and the absorption line for the annealed $\text{Fe}_{0.70}\text{Si}_{0.30}$ alloy film becomes broader, while for the $\text{Fe}_{0.61}\text{Si}_{0.39}$ film it becomes narrower. The changes in the linewidth (as well as in H_s) reflect the increase in perpendicular magnetic anisotropy for the $\text{Fe}_{0.70}\text{Si}_{0.30}$ alloy film possibly owing to the formation of columnar structure and its decrease for the sample $\text{Fe}_{0.61}\text{Si}_{0.39}$.

The structural dependence of the saturation magnetization for nanocrystalline $\text{Fe}_{1-x}\text{Si}_x$ alloys was also observed by Zhou *et al.*;²³ the better the crystallinity, the larger the magnetization. According to Zhou *et al.*, both imperfections inside the grains and grain boundaries result in low magnetization of nanocrystalline Fe-Si alloy films. Thus, the enhancement of the saturation magnetization for our annealed $\text{Fe}_{1-x}\text{Si}_x$ alloy films may be due to some improvement of crystallinity. In addition to this mechanism the enhancement of the saturation magnetization, as well as changes in coercivity, in the annealed state may be explained by some structural and hence magnetic transformations (see below).

According to the Ostwald's rule, a metastable system going to the equilibrium state has to come through the states of intermediate stability.²⁴ A correlation between atomic structure of liquid Fe-Si alloys and peculiarities of the phase diagram was established by Il'inskii *et al.*²⁵ According to this phase diagram the formation of the Fe_3Si and FeSi clusters near the corresponding compositions ($x=0.25$ and 0.50) in the liquid state was experimentally proven.²⁵ Furthermore, an EXAFS study of the nanocrystalline and amorphous $\text{Fe}_{1-x}\text{Si}_x$ alloy films by Díaz *et al.*¹⁴ reveals that the local environment in amorphous phase at each Si concentration corresponds to the simplest crystalline phase of alloy for such a concentration. Thus, using the phase diagram for bulk Fe-Si alloys and coming from the liquid state down the temperature scale along the composition corresponding to $\text{Fe}_{0.70}\text{Si}_{0.30}$ one can find first an amorphous phase (as an analogue of liquid state), then a more stable structure, i.e., a mixture of metastable at RT η phase and stable α_1 phase

may be observed, and eventually, a mixture of both stable ferromagnetic α_1 and nonmagnetic ϵ phases at RT will accomplish the way to the equilibrium state. For $\text{Fe}_{0.61}\text{Si}_{0.39}$ alloy the sequence of possible phases is assumed to be as follows; amorphous phase, then a mixture of metastable β phase and stable ϵ phase at RT, the next step to stability will be a mixture of metastable η phase and stable ϵ phase at RT, and finally (as for the case of $\text{Fe}_{0.70}\text{Si}_{0.30}$ alloy) a mixture of both stable α_1 phase and ϵ phases at RT. The difference between them is ascribed to the different contents of α_1 and ϵ phases in alloy. According to the phase diagram the $\text{Fe}_{0.51}\text{Si}_{0.49}$ alloy should be nonmagnetic after crystallization to ϵ phase. However, due to compositional gradient (of about 10% per sample width) the actual path to the equilibrium state may be the same as for $\text{Fe}_{0.61}\text{Si}_{0.39}$ but with another ratio of the formed stable phases at least for the iron-rich side of this sample. Thus, the significant decrease in coercivity for the $\text{Fe}_{0.61}\text{Si}_{0.39}$ alloy due to annealing may be explained, for example, by the structural transformation from the state with an intermediate stability (mixture of η and ϵ phases, where the magnetically hard η phase is the dominant phase) to an equilibrium state (a mixture of stable α_1 and ϵ phases). Insignificant changes in H_c for the as-deposited and annealed $\text{Fe}_{0.70}\text{Si}_{0.30}$ alloy films may be explained by the fact that in both states (metastable and stable) the magnetically soft α_1 phase is the dominant phase.

The enhancement of magnetization of $\text{Fe}_{1-x}\text{Si}_x$ alloy films upon annealing also may be explained with the help of the phase diagram. For the $\text{Fe}_{1-x}\text{Si}_x$ alloy films with $x=0.30$ (or 0.39) the total magnetization for the last step before equilibrium one may be expressed as $M_{\text{Fe}_{0.70}\text{Si}_{0.30}}^i = M_{\alpha_1} \times C_{\alpha_1}^i(0.30) + M_{\eta} \times C_{\eta}^i(0.30)$ [or $M_{\text{Fe}_{0.61}\text{Si}_{0.39}}^i = M_{\eta} \times C_{\eta}^i(0.39) + M_{\epsilon} \times C_{\epsilon}^i(0.39)$] where M_{α_1} , M_{η} , and M_{ϵ} are magnetization of the α_1 , η , and ϵ phases, respectively, C_{α_1} , C_{η} , and C_{ϵ} are their contents in the state with an intermediate stability. After the structural transformation of alloys to the stable configuration their resulting magnetization may be written as $M_{\text{Fe}_{0.70}\text{Si}_{0.30}}^s = M_{\alpha_1} \times C_{\alpha_1}^s(0.30) + M_{\epsilon} \times C_{\epsilon}^s(0.30)$ [or $M_{\text{Fe}_{0.61}\text{Si}_{0.39}}^s = M_{\alpha_1} \times C_{\alpha_1}^s(0.39) + M_{\epsilon} \times C_{\epsilon}^s(0.39)$]. It should be reminded here that, in contrast to the phase diagram, all the events in such a discussion take place at RT. Because of $C_{\alpha_1}^s \gg C_{\alpha_1}^i$ for $x=0.30$ (as well as for $x=0.39$, see phase diagram) and $M_{\alpha_1} > M_{\eta}$ the $M_{\text{alloy}}^s > M_{\text{alloy}}^i$ even though ϵ phase is nonmagnetic ($M_{\epsilon}=0$). In such an estimation the saturation magnetization for the nanocrystalline $\text{Fe}_{0.75}\text{Si}_{0.25}$ and $\text{Fe}_{0.625}\text{Si}_{0.375}$ ribbons of $1.6\mu_B$ and $0.7\mu_B$, respectively, were used.²⁶

Thus, our magnetic measurements suggest that the cubic phases (DO_3 or $B2$) are dominant phases for the as-deposited and annealed $\text{Fe}_{1-x}\text{Si}_x$ alloy films with $0.21 \leq x \leq 0.30$. A significant amount of the magnetically hard η phase is present in the as-deposited $\text{Fe}_{1-x}\text{Si}_x$ alloy films with $0.39 \leq x \leq 0.49$. Annealing of latter films causes the structural transformation of $\eta + \epsilon \rightarrow \alpha_1 + \epsilon$ type which explains the enhancement of magnetization and decrease in coercivity of these samples.

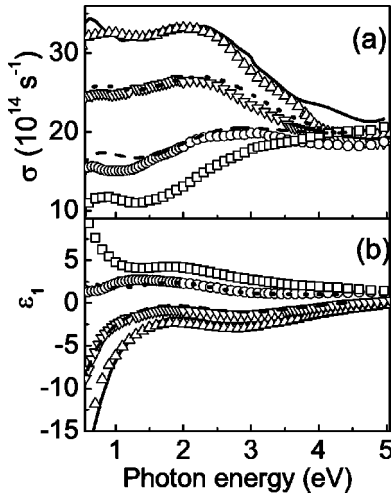


FIG. 4. Experimental (a) OC and (b) ϵ_1 spectra for the as-deposited $\text{Fe}_{1-x}\text{Si}_x$ alloy films with $x=0.21$ (up triangle), 0.30 (down triangle), 0.39 (circle), and 0.49 (square). Both pure-Fe spectrum (solid line) and fitted spectra (dashed and dotted line) are shown.

B. Optical properties of $\text{Fe}_{1-x}\text{Si}_x$ alloy films

$\sigma(\hbar\omega)$ and $\epsilon_1(\hbar\omega)$ spectra of the as-deposited $\text{Fe}_{1-x}\text{Si}_x$ alloy films ($0.21 \leq x \leq 0.49$) together with those of pure Fe-film⁹ are shown in Fig. 4. It is seen that the optical properties of pure Fe and Fe-rich $\text{Fe}_{0.79}\text{Si}_{0.21}$ alloy films practically identical to each other exhibiting a prominent absorption peak at 2.2–2.3 eV in the OC spectra. Increase in Si content leads to the decrease in the magnitude of the OC of the $\text{Fe}_{1-x}\text{Si}_x$ alloy films, to some blueshift of the maximum and also to the appearance of a small feature just below 1 eV.

Based on our magnetic measurements and also considering the phase diagram of bulk Fe-Si alloys we are able to conclude that $\text{Fe}_{1-x}\text{Si}_x$ alloy films with $x=0.21$ and 0.49 contain mainly cubic (DO_3) and ϵ -FeSi phases, respectively. This conclusion is further supported by the fact that the OC spectrum for the as-deposited $\text{Fe}_{0.51}\text{Si}_{0.49}$ alloy film is rather similar to those of bulk ϵ -FeSi alloy and annealed (0.4 nm Fe/0.4 nm Si)₁₂₀ MLF, which crystallizes into ϵ -FeSi phase, taken from our previous work⁹ [see panels (c) and (d) in Fig. 5].

A fully satisfactory description of the optical properties of $\text{Fe}_{1-x}\text{Si}_x$ alloy films with $x=0.30$ – 0.39 can be made by means of two-phase model. The components of DF of multiphase system may be expressed in terms of the effective-medium approximation as follows; $\epsilon_{\text{alloy}} = C_I \times \epsilon_I + (1 - C_I) \times \epsilon_{II}$, where C_I is the fraction of alloy in phase I, and ϵ_I and ϵ_{II} are DF for the phases I and II, respectively. This approach is valid when the dimensions of the regions confining these phases are comparable to the skin depth. It is seen that the experimental $\sigma(\hbar\omega)$ and $\epsilon_1(\hbar\omega)$ spectra for $\text{Fe}_{1-x}\text{Si}_x$ alloy films with $x=0.30$ and 0.39 may be reasonably described by this model with $C_I=0.68$ and 0.28 , respectively (see Fig. 4). The obtained results look reasonable for bulk $\text{Fe}_{0.70}\text{Si}_{0.30}$ alloy in terms of the fractions of these phases in different states of alloy and may unexpected for the $\text{Fe}_{0.61}\text{Si}_{0.39}$ alloy. Indeed, according to the results of our magnetic measurements

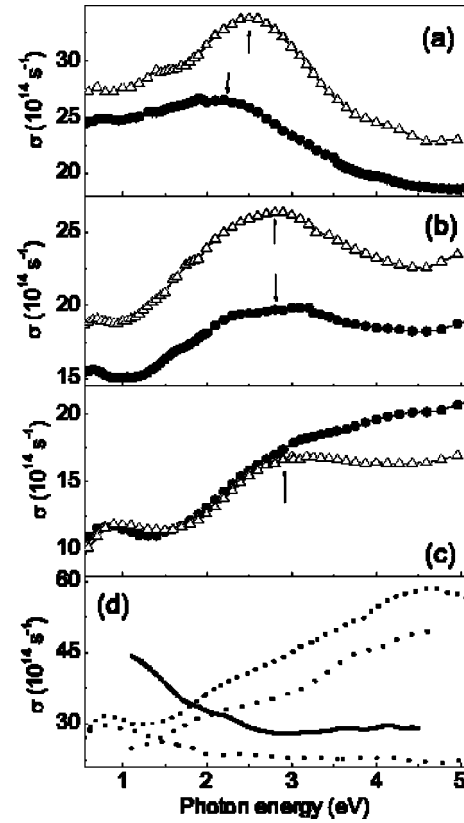


FIG. 5. OC spectra for the as-deposited (solid) and annealed (open) $\text{Fe}_{1-x}\text{Si}_x$ alloy films with (a) $x=0.30$, (b) $x=0.39$, and (c) $x=0.49$. Panel (d) shows the OC spectra extracted from the spontaneously formed silicide in the (30 Å Fe/22 Å Si)₅₀ MLF (solid) and after ion-beam mixing (dashed), annealed (4 Å Fe/4 Å Si)₁₂₀ MLF (dashed-dotted-dotted line), and bulk ϵ -FeSi alloy (dotted).

the η phase should be the dominant phase for $x=0.39$. However, this contradiction may be avoided if some similarity in the optical properties of α_1 ($\text{Fe}_{0.75}\text{Si}_{0.25}$) and η phases ($\text{Fe}_{0.625}\text{Si}_{0.375}$) will be assumed.

Annealing of the $\text{Fe}_{1-x}\text{Si}_x$ alloy films causes noticeable changes in the OC spectra in a somewhat different way for different composition as shown in Fig. 5. While the overall magnitude of the OC spectra increases as a whole owing to the annealing of the alloys with $x=0.30$ and 0.39 , the absorption peak in the OC spectrum of $\text{Fe}_{0.70}\text{Si}_{0.30}$ alloy is blue-shifted by about 0.3 eV, whereas it is almost unchanged for $x=0.39$. After annealing the OC spectrum of $\text{Fe}_{0.51}\text{Si}_{0.49}$ alloy film resembles that of $\text{Fe}_{0.41}\text{Si}_{0.39}$ alloy. According to previous discussions, all annealed $\text{Fe}_{1-x}\text{Si}_x$ alloy films should contain in the equilibrium state a mixture of α_1 and ϵ phases in proportions depending on alloy compositions. The annealing leads to more resemblance in the OC spectra of $\text{Fe}_{1-x}\text{Si}_x$ alloy films; all OC spectra have rather similar shape and exhibit an interband absorption peaks located at 2.5 eV ($x=0.30$), 2.85 eV ($x=0.39$), and 3.1 eV ($x=0.49$). It is also seen that the high-energy shoulder of these peaks for the annealed samples is getting more intense, as the Si content increases (see Fig. 5). The consistent blue-shift of this peak in comparison with that of $\text{Fe}_{0.70}\text{Si}_{0.30}$ (with increase in x) results from the increased contribution from the ϵ -FeSi phase. The absorption peak observed at 2.5–3.1 eV in

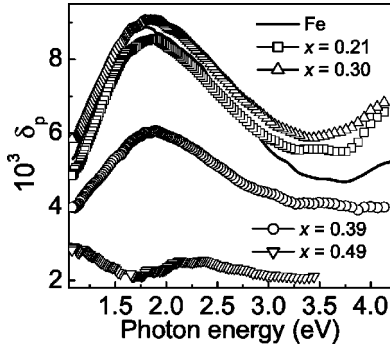


FIG. 6. Experimental EKE spectra for the as-deposited $\text{Fe}_{1-x}\text{Si}_x$ alloy films (symbols) and pure Fe film (Ref. 9) taken at the angle of incidence of $\varphi = 66^\circ$.

the OC spectra of $\text{Fe}_{1-x}\text{Si}_x$ alloys ($x = 0.30\text{--}0.49$) may have the same origin as the 2.4 eV peak of the Fe spectrum. The lattice constant of the α phase rapidly decreases with Si content (see Fig. 2). This process should be accompanied by a “stretching” of the energy bands from the Fermi level, and considering the origin of this peak with its blueshift. However, according to the results of our structural study, the interplanar spacings of the as-deposited $\text{Fe}_{1-x}\text{Si}_x$ alloy films are nearly independent of x . Therefore, the actual nature of the main absorption peak in the OC spectra of α_1 phase may be understood by the results of the first-principles calculations. At the same time the complete diversity between the optical properties of newly obtained $\text{Fe}_{1-x}\text{Si}_x$ alloy films either in the as-deposited or annealed states and those of spontaneously formed spacer in the Fe/Si MLF or the top layer of the ion-beam-mixed one allows us to conclude that the metastable FeSi ($B2$) and Fe_2Si ($B2$) iron silicides cannot be obtained by codeposition of Fe and Si.

C. Magneto-optical properties of $\text{Fe}_{1-x}\text{Si}_x$ alloy films

The EKE spectra for the $\text{Fe}_{1-x}\text{Si}_x$ alloy films in the as-deposited state and after annealing are shown in Figs. 6 and 7. It is seen that $\text{Fe}_{1-x}\text{Si}_x$ alloy films ($x \leq 0.30$) have mainly the cubic structure (DO_3 or bcc) and have the EKE spectra which practically coincide with that of pure Fe film taken from our previous work.⁹ Although the concentrations of Si in these alloys are 21 and 30 at%, the magnitudes of the EKE spectra near 1.7 eV exceed (especially for annealed $\text{Fe}_{0.70}\text{Si}_{0.30}$ alloy film by about 13%) that for pure Fe film (see Figs. 6 and 7). The EKE spectrum for the intermediate region of composition $x = 0.39$ still preserves the similarity in the spectral shape, however, its magnitude is noticeably smaller. The EKE spectrum for the as-deposited $\text{Fe}_{0.51}\text{Si}_{0.49}$ alloy film drastically differs from all the other spectra in its shape and magnitude. Annealing of the $\text{Fe}_{1-x}\text{Si}_x$ alloy films causes some enhancement of the MO response by about 10–15% without significant changes in the spectral shape (see Fig. 7). The enhancement of the magnitude of EKE spectra upon alloying of Fe with Si is somewhat smaller than that observed by Zhou *et al.*¹⁵ for the nanocrystalline alloy films with similar compositions, but the trend is the same.

As well known, the MO response of a medium depends on its off-diagonal and diagonal components of dielectric

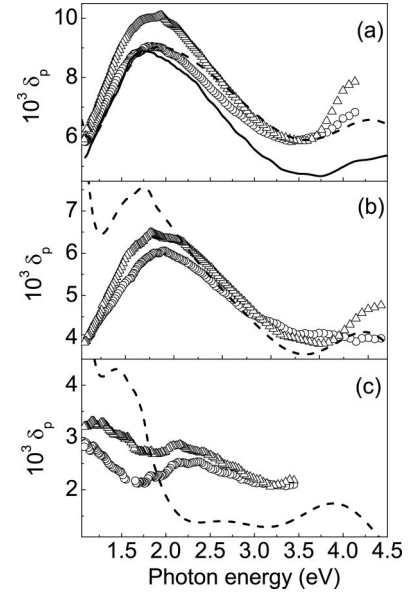


FIG. 7. Experimental EKE spectra of the as-deposited (circle) and annealed (triangle) $\text{Fe}_{1-x}\text{Si}_x$ alloy films with (a) $x = 0.30$, (b) $x = 0.39$, and (c) $x = 0.49$. The EKE spectrum for Fe-film (solid line) and the model EKE spectra (dashed lines) are also shown. The angle of incidence is 66° .

tensor. Therefore, this phenomenon may be caused by the interplay between the optical constants of Fe and $\text{Fe}_{1-x}\text{Si}_x$ alloys and/or by the enhancement of the off-diagonal components of the DF.

In order to elucidate which mechanism is actually responsible for the enhancement, simulations of the EKE spectra for the $\text{Fe}_{1-x}\text{Si}_x$ alloy films have been performed in the framework of the effective-medium approximation. All the cubic phases present in the $\text{Fe}_{1-x}\text{Si}_x$ alloys for $0 \leq x \leq 0.28$ [i.e., α -Fe, α_1 (DO_3), or α_2 phases (bcc)] are based on the bcc lattice. It is also well known that down to $x \approx 0.30$ the saturation magnetization for bulk $\text{Fe}_{1-x}\text{Si}_x$ alloys decreases nearly linearly with the Si content.¹⁹ In the region of solid solutions (up to $x \approx 0.25$) the resulting saturation magnetization (M_s) forms the so-called Slater-Pauling curve.^{18,27} This means that the constituent atoms in Fe-Si alloys still hold their intrinsic properties. All these facts allow us to assume that the nearly linear behavior of exchange-interaction-related parameters (i.e., the off-diagonal components of DF) will also decrease nearly linearly with x .

The transverse or equatorial Kerr effect in a medium observed at the angle of incidence φ can be expressed in terms of the diagonal ($\tilde{\epsilon} = \tilde{\epsilon}_{xx} = \tilde{\epsilon}_{yy} = \epsilon_1 + i\epsilon_2$) and off-diagonal ($\tilde{\epsilon}_{xy} = -\tilde{\epsilon}_{yx} = i\tilde{\epsilon}'$; $\tilde{\epsilon}' = \epsilon_1' - i\epsilon_2'$) components of its DF as²⁸

$$\delta_p = 2 \sin 2\varphi \times \left(\frac{A \times \epsilon_1'}{A^2 + B^2} + \frac{B \times \epsilon_2'}{A^2 + B^2} \right),$$

where

$$A = \epsilon_2 \times (2\epsilon_1 \times \cos^2 \varphi - 1),$$

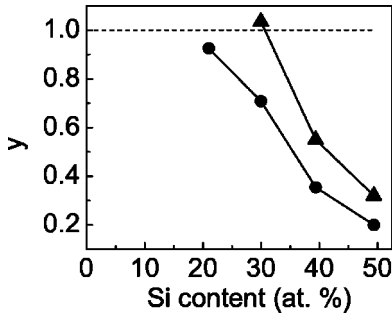


FIG. 8. Compositional dependence of the y coefficient for the as-deposited (circle) and annealed (triangle) $\text{Fe}_{1-x}\text{Si}_x$ alloy films.

$$B = (\varepsilon_2^2 - \varepsilon_1^2) \times \cos^2 \varphi + \varepsilon_1 - \sin^2 \varphi.$$

In our model the scaled off-diagonal components of pure Fe were chosen as those for the DF of the $\text{Fe}_{1-x}\text{Si}_x$ alloy films, i.e., $\varepsilon'_{1,2(\text{Fe}_{1-x}\text{Si}_x)} = f(x) \times \varepsilon'_{1,2(\text{Fe})}$, where $f(x)$ is a scaling factor. The measured optical constants of $\text{Fe}_{1-x}\text{Si}_x$ alloy films were used in the model as the diagonal components of the DF. The simulated spectra for $\text{Fe}_{0.79}\text{Si}_{0.21}$ (not shown) and $\text{Fe}_{0.70}\text{Si}_{0.30}$ [see Fig. 7(a)] nicely reproduce the experimental spectra for the as-deposited alloy films. The simulated EKE spectrum for the $\text{Fe}_{0.61}\text{Si}_{0.39}$ alloy film also reasonably describes the experimental one, but with less confidence [see Fig. 7(b)]. Furthermore, the resemblance between the experimental and simulated spectra for the $\text{Fe}_{0.51}\text{Si}_{0.49}$ alloy film is completely lost [see Fig. 7(c)]. For the region of linear decrease in magnetization the scaling factor $f(x)$ is expected to be equal to $(1-x)$. However, in order to fit the magnitudes of the modeled and experimental EKE spectra the scaling factors $f(x)$ were found to be somewhat smaller than corresponding values of $(1-x)$, and the higher the Si content in alloy, the larger the deviation. Its compositional dependence may be expressed as $f(x) = (1-x) \times y(x)$, where $y(x)$ is another fitting parameter. Figure 8 shows the compositional dependence of the function $y(x)$ for the $\text{Fe}_{1-x}\text{Si}_x$ alloy films in the as-deposited and annealed states. The crossing of the $y(x)$ curve and $y=1$ line occurs at $x \approx 0.20$ and $x \approx 0.30$ for the as-deposited and annealed states, respectively. It means that the region, where the Slater-Pauling curve is still valid, is restricted by $x \approx 0.20$ and $x \approx 0.30$ for the as-deposited and annealed states, respectively. This may manifest the enrichment of the cubic DO_3 phase in the annealed films.

Thus, it is clear that the experimentally observed enhancement of the MO response for $\text{Fe}_{1-x}\text{Si}_x$ alloy films with $0.20 \leq x \leq 0.30$ in comparison with that of pure Fe film is a result of interplay between the optical constants of Fe and $\text{Fe}_{1-x}\text{Si}_x$ alloy films. The deviation from linear decrease in the magnetization with increase in x and occurrence of the

plateau of constant magnetization for the nanocrystalline $\text{Fe}_{1-x}\text{Si}_x$ alloys in $0.2 < x < 0.3$ region observed by Zhou *et al.*¹⁵ and Díaz *et al.*¹⁴ may have the same origin (i.e., interplay of the optical constants) and should be considered as an artifact, because these measurements have been performed by using MO tool. At the same time, the disagreement between the shape of the experimental and simulated spectra for $\text{Fe}_{1-x}\text{Si}_x$ alloy films with $x = 0.49$ (and partly for $x = 0.39$) allows us to presume that another noncubic phase is the dominant phase in $\text{Fe}_{1-x}\text{Si}_x$ alloy films in this compositional region.

IV. CONCLUSIONS

A set of nanocrystalline and amorphous $\text{Fe}_{1-x}\text{Si}_x$ alloy films with $0 < x < 1$ have been prepared by dc magnetron sputtering and their magnetic, optical and MO properties were investigated for the $0 < x \leq 0.5$ compositional range. By analyzing the magnetic properties we can indirectly determine the structures of the $\text{Fe}_{1-x}\text{Si}_x$ alloy films. According to this approach the cubic structures (DO_3 or bcc) are formed in the $\text{Fe}_{1-x}\text{Si}_x$ alloy films with $x \leq 0.30$, while some trace of hexagonal $\eta\text{-Fe}_5\text{Si}_3$ is present in $0.30 < x < 0.50$ region. Annealing of the films causes noticeable changes in their magnetic properties. Most of these changes may be explained by the enrichment of the cubic DO_3 phase in the films.

The optical properties of nanocrystalline and amorphous $\text{Fe}_{1-x}\text{Si}_x$ alloy films with $0.21 \leq x \leq 0.49$ were firstly investigated. The OC spectrum of the amorphous $\text{Fe}_{0.51}\text{Si}_{0.49}$ alloy film shows the great resemblance with the OC spectrum of crystalline $\epsilon\text{-FeSi}$ ($B20$), implying that the same type of short-range order is formed in this amorphous structure. Annealing of the $\text{Fe}_{1-x}\text{Si}_x$ alloy films results in the increase of the resemblance between the OC spectra for all films (i.e., causes the formation of the prominent absorption peak near 2.5–3.1 eV) presumably due to the formation of same phases in the equilibrium state of alloys, but with a different contents of these phases. For $0.21 \leq x \leq 0.30$ compositional range the MO responses of $\text{Fe}_{1-x}\text{Si}_x$ alloy films exceed that of pure Fe films. Such an enhancement is due to the interplay between the optical properties of Fe and $\text{Fe}_{1-x}\text{Si}_x$ alloy films.

We were not able to fabricate the metastable FeSi ($B2$) and Fe_2Si ($B2$) alloy films by using codeposition of Fe and Si and post-heat treatment. This may be explained by specific growth conditions of the iron-silicide phases embedded between Fe and Si sublayers.

ACKNOWLEDGMENTS

This work was supported by the Korea Science and Engineering Foundation through the Quantum Photonic Science Research Center, and by the Korea Research Foundation (Grant Nos. KRF-99-D00048 and KRF-01-DP0193).

*Electronic address: yplee@hanyang.ac.kr

¹Binary Alloy Phase Diagrams, edited by T.B. Massalski (American Society for Metals, 1986), Vol. I, p. 1100.

²P. Veillars and L.D. Calvert, *Pearson's Handbook of Crystallographic Data for Intermetallic Phases* (American Society for

Metals, Metal Park, OH, 1985).

³H. von Känel, K.A. Mäder, E. Müller, N. Onda, and H. Sirringhaus, *Phys. Rev. B* **45**, 13 807 (1992).

⁴J.A. Carlisle, A. Chaiken, R.P. Michel, L.J. Terminello, J.J. Jia, T.A. Callcott, and D.L. Ederer, *Phys. Rev. B* **53**, R8824 (1996).

- ⁵E.E. Fullerton, J.E. Mattson, S.R. Lee, C.H. Sowers, Y.Y. Huang, G. Felcher, S.D. Bader, and F.T. Parker, *J. Appl. Phys.* **73**, 6335 (1993).
- ⁶G.J. Strijkers, J.T. Kohlhepp, H.J.M. Swagten, and W.J.M. de Jonge, *Phys. Rev. B* **60**, 9583 (1999).
- ⁷J.J. de Vries, J. Kohlhepp, F.J.A. den Broeder, R. Coehoorn, R. Jungblut, A. Reinders, and W.J.M. de Jonge, *Phys. Rev. Lett.* **78**, 3023 (1997).
- ⁸A. Chaiken, R.P. Michel, and M.A. Wall, *Phys. Rev. B* **53**, 5518 (1995).
- ⁹Y.V. Kudryavtsev, V.V. Nemoshkalkenko, Y.P. Lee, K.W. Kim, J.Y. Rhee, and J. Dubowik, *J. Appl. Phys.* **90**, 2903 (2001).
- ¹⁰Y.V. Kudryavtsev, Y.P. Lee, J. Dubowik, B. Szymański, and J.Y. Rhee, *Phys. Rev. B* **65**, 104417 (2002).
- ¹¹E.G. Michel, *Appl. Surf. Sci.* **117/118**, 294 (1997).
- ¹²A. Gupta and P. Dhuri, *Mater. Sci. Eng., A* **304-305**, 394 (2001).
- ¹³L. Tie, Y.Z. Li, and Y.H. Zhang, *J. Phys.: Condens. Matter* **9**, 1381 (1997).
- ¹⁴J. Díaz, S.M. Valvidares, R. Morales, and J.M. Alameda, *J. Magn. Mater.* **242-245**, 166 (2002).
- ¹⁵T.J. Zhou, W. Yang, Z. Yu, H.H. Zhang, J.C. Shen, and Y.W. Du, *Appl. Phys. Lett.* **72**, 1383 (1998).
- ¹⁶V.N. Antonov, W. Henrion, M. Rebien, P. Stauß, H. Lange, and O. Jepsen, *Phys. Rev. B* **57**, 8934 (1998), and reference therein; Z. Schlesinger, Z. Fisk, Hai-Tao Zhang, and M.B. Maple, *Physica B* **237-238**, 460 (1997), and references therein; H. Lange, *Thin Solid Films* **381**, 171 (2001).
- ¹⁷Yu.V. Kudryavtsev, Y.P. Lee, and K.W. Kim, *J. Appl. Phys.* **83**, 1575 (1998).
- ¹⁸N.I. Kulikov, D. Fristot, A. Postnikov, and J. Hugel, *Comput. Mater. Sci.* **17**, 196 (2000).
- ¹⁹R.M. Bozorth, *Ferromagnetism* (IEEE Press, New York, 1993), p. 717.
- ²⁰T.J. Zhou, Z. Yu, and Y.W. Du, *J. Magn. Mater.* **202**, 354 (1999).
- ²¹L.K. Varga, F. Mazaleyrat, J. Kovac, and A. Kákay, *J. Magn. Mater.* **215-216**, 121 (2000).
- ²²M. Vélez, R. Morales, J.M. Alameda, F. Briones, J.I. Martin, and J.L. Vincent, *J. Appl. Phys.* **87**, 5654 (2000).
- ²³T.J. Zhou, Z. Yu, and Y.W. Du, *Appl. Phys. A: Mater. Sci. Process.* **70**, 75 (2000).
- ²⁴A.F. Hollemann and E. Wiberg, *Lehrbuch der Anorganischen Chemie*, 71-80th ed. (Walter de Gruyter, Berlin, 1971).
- ²⁵A. Il'inskii, S. Slyusarenko, O. Slikhovskii, I. Kaban, and W. Hoyer, *J. Non-Cryst. Solids* **306**, 90 (2002).
- ²⁶L.K. Varga, F. Mazaleyrat, J. Kovac, and A. Kákay, *Mater. Sci. Eng., A* **304-306**, 946 (2001).
- ²⁷J. Kudrnovský, N.E. Christensen, and O.K. Andersen, *Phys. Rev. B* **43**, 5924 (1991).
- ²⁸G.S. Krinchik, *Physics of Magnetic Phenomena* (MGU, Moscow, 1976) (in Russian).
- ²⁹W.B. Pearson, *Handbook of Lattice Spacing and Structures of Metals and Alloys* (Pergamon, Oxford, 1958).